

Coherent intraband and interband dynamics in double quantum wells: Exciton and free-carrier effects

E. Binder, T. Kuhn, and G. Mahler

Institut für Theoretische Physik, Universität Stuttgart, Pfaffenwaldring 57, 70550 Stuttgart, Germany

(Received 12 July 1994)

Exciton energies and eigenfunctions in asymmetric double quantum wells are calculated as functions of an applied electric field. From these data, absorption spectra are calculated and the localization behavior of the excitonic states is investigated. The coherent dynamics in asymmetric double quantum wells, which is strongly influenced by excitonic effects, is analyzed by a numerical solution of the multisubband semiconductor Bloch equations. Under resonance conditions the oscillating dipole moment leads to a coherent terahertz emission. In general, the spectrum of this radiation has contributions due to both, the free-carrier and exciton energies, the details being determined by the excitation and dephasing conditions. The calculated absorption spectra and the frequency of the terahertz radiation are in good agreement with recent experiments.

I. INTRODUCTION

As the time scales accessible by experiments continue to shrink, coherent aspects in the dynamics of photoexcited semiconductors have become of growing interest during the past few years. Many results have been achieved by performing four-wave-mixing experiments, where a third-order nonlinearity of the excited semiconductor is used to generate a signal in a background-free direction. Various phenomena include photon echo,¹⁻⁵ quantum beats,⁶⁻⁸ the dynamics of wave packets,⁹ tunneling dynamics,¹⁰ and many-body effects,^{5,11-13} both in bulk semiconductors and heterostructures.

While in a bulk semiconductor, the dynamics is governed mainly by material parameters, heterostructures offer the additional possibility of tuning properties by band-gap engineering. Of particular interest are multiple-quantum-well structures: Due to the possibility to control the localization behavior of the carrier states by an externally applied electric field, they allow for interesting phenomena like anticrossing effects related to resonances,^{14,15} charge transfer between the wells,^{14,16,17} and coherent oscillations.¹⁸

In an experiment measuring third-order nonlinearities, the frequency of the emitted signal is typically of the same order of magnitude as the excitation frequency. In contrast, second-order nonlinearities, being related to sum or difference frequencies, occur in strongly different frequency ranges. In a homogeneous semiconductor such second-order optical nonlinearities often are small or even vanish for symmetry reasons. They can strongly be enhanced by spatial inhomogeneities¹⁹ and may then lead to the emission of electromagnetic radiation with a frequency much lower than the excitation frequency. Such an emission in the terahertz range has recently been observed and analyzed theoretically in various geometries, where the inhomogeneity is due to a surface,²⁰ a single quantum well,²¹⁻²³ a double quantum well,²²⁻²⁶ or a superlattice.^{23,27} Surprisingly, the measured frequency

of the radiation, in particular, in the case of the double quantum well, did not coincide with the difference between the two lowest exciton states, as would be expected in a three-level model.²⁴ However, by using the full multisubband semiconductor Bloch equations, we have found the absorption spectrum, i.e., the energies and oscillator strengths of the excitons, as well as the frequency of the terahertz radiation to be in good agreement with the experiment.²⁸ In that work, however, we did not give any explanation of the various frequency components entering the signal.

The aim of this paper is to present a detailed discussion of the role played by excitons and free carriers for the spectral properties of the terahertz radiation emitted from an asymmetric double quantum well. We will show that, in general, both, exciton and free-carrier energies, contribute to the spectrum, the shape being strongly influenced by details of the dephasing processes.²⁹ The calculations are based on the semiconductor Bloch equations for a multisubband system,^{28,30,31} which are analyzed both in a free-carrier and an exciton representation.

The paper is organized as follows: In Sec. II, we introduce the model describing the semiconductor interacting with a coherent light field. Carrier-carrier interaction, which is responsible for the excitonic effects, is included in the Hamiltonian. We derive the equations of motion describing the coherent dynamics in a quantum-well heterostructure, i.e., the multisubband semiconductor Bloch equations. Section III addresses different aspects. We first investigate static properties of the system as the basis for understanding the dynamics. In Sec. III A, we calculate exciton eigenstates and eigenvectors of an asymmetric double-quantum-well heterostructure as functions of an applied electric field. We discuss the resonance (anticrossing) effects induced by the field and the localization behavior of the excitons which is different from that of free carriers. In Sec. III B, we present the absorption spectra as functions of the applied field. Section III C is devoted to charge oscillations due to the

generation of a superposition of states. In Sec. III D, we derive the equations describing the terahertz radiation of a heterostructure and present numerical results. We discuss in detail the various frequency components entering the signal and the role played by dephasing processes. Finally, in Sec. IV, we draw some conclusions.

II. THEORETICAL MODEL

In this section, we derive the equations of motion describing the coherent dynamics in a quantum-well heterostructure.^{30,31} The treatment is a multisubband generalization of the bulk case.^{32–36} To describe the semiconductor heterostructure, we use the effective mass approximation within the envelope-function approximation and consider two isotropic parabolic bands, the conduction band and the heavy hole valence band. We thus neglect any effects related to light holes, valence band mixing, and nonparabolicity. These effects, so far, have been extensively studied only for the static case.^{37,38} Effects of valence band mixing on the dynamics have been reported in Ref. 31.

In a quantum-well heterostructure the motion of carriers in one direction (the growth or z direction) is quantized, while in the other two dimensions the motion is free. The carrier states are then characterized by a discrete subband index i or j and a continuous two-dimensional wave vector \mathbf{k} . Here, as in the following, an index i refers to an electron subband and j to a hole subband. In the envelope-function approximation the wave functions for the conduction band ($\psi_{i,\mathbf{k}}^C(\mathbf{R})$) and the valence band ($\psi_{j,\mathbf{k}}^V(\mathbf{R})$) states are given by

$$\psi_{i,\mathbf{k}}^C(\mathbf{R}) = \frac{1}{\sqrt{A}} e^{i\mathbf{k}\cdot\mathbf{r}} \phi_i(z) u_0^C(\mathbf{R}), \quad (1a)$$

$$\psi_{j,\mathbf{k}}^V(\mathbf{R}) = \frac{1}{\sqrt{A}} e^{i\mathbf{k}\cdot\mathbf{r}} \phi_j(z) u_0^V(\mathbf{R}), \quad (1b)$$

where $\mathbf{R} = (x, y, z)$ is a three-dimensional position vector, $\mathbf{r} = (x, y)$ is the corresponding two-dimensional in-plane vector perpendicular to the growth direction, \mathbf{k} is

the two-dimensional in-plane wave vector, $u_0^{C,V}(\mathbf{R})$ are the lattice-periodic Bloch functions at the band extrema, A is a normalization area, and ϕ_i and ϕ_j are the envelope functions along the growth direction.

The single-particle Hamiltonian in an electron-hole picture, including the coupling to a classical light field, is given by

$$\begin{aligned} H_0 = & \sum_i \sum_{\mathbf{k}} \epsilon_{i,\mathbf{k}}^e c_{i,\mathbf{k}}^\dagger c_{i,\mathbf{k}} + \sum_j \sum_{\mathbf{k}} \epsilon_{j,\mathbf{k}}^h d_{j,\mathbf{k}}^\dagger d_{j,\mathbf{k}} \\ & + \sum_{i,j} \sum_{\mathbf{k}} [\mathbf{M}_{ij,\mathbf{k}}^{eh} \cdot \mathbf{E}^{(+)}(t) c_{i,\mathbf{k}}^\dagger d_{j,-\mathbf{k}}^\dagger \\ & + \mathbf{M}_{ij,\mathbf{k}}^{eh*} \cdot \mathbf{E}^{(-)}(t) d_{j,-\mathbf{k}} c_{i,\mathbf{k}}] . \end{aligned} \quad (2)$$

Here, $c_{i,\mathbf{k}}^\dagger, d_{j,\mathbf{k}}^\dagger$ ($c_{i,\mathbf{k}}, d_{j,\mathbf{k}}$) denote creation (annihilation) operators of electrons and holes and $\epsilon_{i,\mathbf{k}}^e$ and $\epsilon_{j,\mathbf{k}}^h$ the corresponding energies of electron and hole states. The external light field is given in terms of the positive (negative) frequency part of the electric field $\mathbf{E}^{(+)} (\mathbf{E}^{(-)})$ with

$$\mathbf{E}^{(+)} = \mathbf{e}_L E_0(t) e^{-i\omega_L t}, \quad \mathbf{E}^{(-)} = \mathbf{E}^{(+)*}, \quad (3)$$

the central angular frequency ω_L , the polarization unit vector \mathbf{e}_L , a pulse shape given by $E_0(t)$, and the coupling is treated in rotating-wave approximation. For the numerical applications, we will use a Gaussian pulse $E_0(t) = E_L \exp[-(t/\tau_L)^2]$. In the envelope-function approximation, where the lattice-periodic part of the wave function is assumed to be independent of the material, the interband dipole matrix element is directly related to the bulk case. Neglecting the wave vector dependence of the bulk dipole matrix element \mathbf{M}_0 , the quantum-well matrix element is given by

$$\mathbf{M}_{ij,\mathbf{k}}^{eh} = \mathbf{M}_0 \int \phi_i^*(z) \phi_j(z) dz . \quad (4)$$

To describe excitonic effects which completely determine the optical properties of a semiconductor in a region close to the gap, we have to include carrier-carrier interaction. The corresponding Hamiltonian is given by^{30,39}

$$\begin{aligned} H_{cc} = & \frac{1}{2} \sum_{i_1, i_2, i_3, i_4} \sum_{\mathbf{k}, \mathbf{k}', \mathbf{q}} V_{i_1 i_2 i_3 i_4}(\mathbf{q}) c_{i_1, \mathbf{k}+\mathbf{q}}^\dagger c_{i_2, \mathbf{k}'-\mathbf{q}}^\dagger c_{i_3, \mathbf{k}'} c_{i_4, \mathbf{k}} + \frac{1}{2} \sum_{j_1, j_2, j_3, j_4} \sum_{\mathbf{k}, \mathbf{k}', \mathbf{q}} V_{j_4 j_3 j_2 j_1}(\mathbf{q}) d_{j_1, \mathbf{k}+\mathbf{q}}^\dagger d_{j_2, \mathbf{k}'-\mathbf{q}}^\dagger d_{j_3, \mathbf{k}'} d_{j_4, \mathbf{k}} \\ & - \sum_{i_1, i_2, j_1, j_2} \sum_{\mathbf{k}, \mathbf{k}', \mathbf{q}} V_{i_1 j_2 j_1 i_2}(\mathbf{q}) c_{i_1, \mathbf{k}+\mathbf{q}}^\dagger d_{j_1, \mathbf{k}'-\mathbf{q}}^\dagger d_{j_2, \mathbf{k}'} c_{i_2, \mathbf{k}}, \end{aligned} \quad (5)$$

with the Coulomb matrix element

$$\begin{aligned} V_{n_1 n_2 n_3 n_4}(\mathbf{q}) = & \frac{2\pi e^2}{\epsilon_s A q} \iint \phi_{n_1}^*(z) \phi_{n_2}^*(z') e^{-q|z-z'|} \\ & \times \phi_{n_3}(z) \phi_{n_4}(z) dz dz', \end{aligned} \quad (6)$$

where n_i refers to both electron and hole subbands and

ϵ_s is the static dielectric constant. We have neglected the interband exchange interaction, as is usually done in the case where the exciton binding energy is small compared to the band gap.⁴⁰ All intersubband exchange terms, however, are taken into account.

The basic variables to describe the dynamics are the single-particle density matrices.³⁰ They are given by the interband density matrices

$$p_{ji,\mathbf{k}} = \langle d_{j,-\mathbf{k}} c_{i,\mathbf{k}} \rangle \quad \text{and} \quad p_{ji,\mathbf{k}}^* = \langle c_{i,\mathbf{k}}^\dagger d_{j,-\mathbf{k}}^\dagger \rangle, \quad (7)$$

which describe the interband polarization, and the intra-band density matrices of electrons and holes,

$$f_{i_1 i_2, \mathbf{k}}^e = \langle c_{i_1, \mathbf{k}}^\dagger c_{i_2, \mathbf{k}} \rangle \quad \text{and} \quad f_{j_1 j_2, \mathbf{k}}^h = \langle d_{j_1, \mathbf{k}}^\dagger d_{j_2, \mathbf{k}} \rangle. \quad (8)$$

The diagonal components of the latter variables are the distribution functions, while the off-diagonal components, the intraband polarizations, describe the coherence between different subbands.

With respect to the Hamiltonian H_0 , these variables satisfy a closed set of equations of motion. Carrier-carrier interaction, however, introduces correlations leading to an infinite hierarchy of equations for n -particle density matrices. In this paper we concentrate on an excitation close to the band gap and to the case of low densities. We take into account only the first-order terms in carrier-carrier interaction, i.e., we limit ourselves to the Hartree-Fock approximation.^{30,32,34,40} In this case, electron-electron and hole-hole interaction lead to self-energy matrices,

$$\hbar\Omega_{i_1 i_2, \mathbf{k}}^e = - \sum_{i_3 i_4} \sum_{\mathbf{k}'} V_{i_1 i_3 i_2 i_4}(\mathbf{k} - \mathbf{k}') f_{i_3 i_4, \mathbf{k}'}^e, \quad (9a)$$

$$\hbar\Omega_{j_1 j_2, \mathbf{k}}^h = - \sum_{j_3 j_4} \sum_{\mathbf{k}'} V_{j_2 j_4 j_1 j_3}(\mathbf{k} - \mathbf{k}') f_{j_3 j_4, \mathbf{k}'}^h, \quad (9b)$$

which renormalize the free-carrier energies resulting in the renormalized energy matrices,

$$\mathcal{E}_{i_1 i_2, \mathbf{k}}^e = \epsilon_{i_1, \mathbf{k}}^e \delta_{i_1 i_2} + \hbar\Omega_{i_1 i_2, \mathbf{k}}^e, \quad (10a)$$

$$\mathcal{E}_{j_1 j_2, \mathbf{k}}^h = \epsilon_{j_1, \mathbf{k}}^h \delta_{j_1 j_2} + \hbar\Omega_{j_1 j_2, \mathbf{k}}^h. \quad (10b)$$

The effect of electron-hole interaction can be expressed in terms of an internal field matrix,

$$\Delta_{i_1 j_1, \mathbf{k}} = - \sum_{i_2 j_2} \sum_{\mathbf{k}'} V_{i_1 j_2 j_1 i_2}(\mathbf{k} - \mathbf{k}') p_{j_2 i_2, \mathbf{k}'} \quad (11)$$

which renormalizes the external field resulting in the effective field matrix,

$$\mathcal{U}_{i_1 j_1, \mathbf{k}} = \mathbf{M}_{i_1 j_1, \mathbf{k}}^{eh} \cdot \mathbf{E}^{(+)}(t) + \Delta_{i_1 j_1, \mathbf{k}}. \quad (12)$$

Using the Heisenberg equation of motion, we can derive the equations of motion for the various single-particle density matrices. They are given by

$$\begin{aligned} \frac{d}{dt} f_{i_1 i_2, \mathbf{k}}^e &= \frac{1}{i\hbar} \sum_{i_3 i_4} (\mathcal{E}_{i_2 i_4, \mathbf{k}}^e \delta_{i_1 i_3} - \mathcal{E}_{i_3 i_1, \mathbf{k}}^e \delta_{i_2 i_4}) f_{i_3 i_4, \mathbf{k}}^e \\ &+ \frac{1}{i\hbar} \sum_{j_1} (\mathcal{U}_{i_2 j_1, \mathbf{k}} p_{j_1 i_1, \mathbf{k}}^* - \mathcal{U}_{i_1 j_1, \mathbf{k}}^* p_{j_1 i_2, \mathbf{k}}), \end{aligned} \quad (13a)$$

$$\begin{aligned} \frac{d}{dt} f_{j_1 j_2, -\mathbf{k}}^h &= \frac{1}{i\hbar} \sum_{j_3 j_4} (\mathcal{E}_{j_2 j_4, -\mathbf{k}}^h \delta_{j_1 j_3} - \mathcal{E}_{j_3 j_1, -\mathbf{k}}^h \delta_{j_2 j_4}) f_{j_3 j_4, -\mathbf{k}}^h \\ &+ \frac{1}{i\hbar} \sum_{i_1} (\mathcal{U}_{i_1 j_2, \mathbf{k}} p_{j_1 i_1, \mathbf{k}}^* - \mathcal{U}_{i_1 j_1, \mathbf{k}}^* p_{j_2 i_1, \mathbf{k}}), \end{aligned} \quad (13b)$$

$$\begin{aligned} \frac{d}{dt} p_{j_1 i_1, \mathbf{k}} &= \frac{1}{i\hbar} \sum_{i_2 j_2} (\mathcal{E}_{j_1 j_2, -\mathbf{k}}^h \delta_{i_1 i_2} + \mathcal{E}_{i_1 i_2, \mathbf{k}}^e \delta_{j_1 j_2}) p_{j_2 i_2, \mathbf{k}} \\ &+ \mathcal{U}_{i_2 j_2, \mathbf{k}} (\delta_{i_1 i_2} \delta_{j_1 j_2} - \delta_{j_1 j_2} f_{i_2 i_1, \mathbf{k}}^e \\ &- \delta_{i_1 i_2} f_{j_2 j_1, -\mathbf{k}}^h). \end{aligned} \quad (13c)$$

These are the multisubband semiconductor Bloch equations without damping terms. Similar equations have been derived in Ref. 31, where a valence band mixing has been included but the off-diagonal parts between different subbands have been neglected.

As already mentioned, here we want to limit ourselves to the case of a sufficiently low excitation. When expanded in powers of the electric field strength, the interband variables have only contributions with odd orders while in the intraband terms only even orders appear. For the purpose of this paper, it is sufficient to take into account only contributions up to second order. Then we can neglect all nonlinearities in the equations of motion related to self-energies as well as the phase-space filling terms in Eq. (13c). We furthermore neglect a screening of the Coulomb potential and obtain the following simplified set of equations:

$$\begin{aligned} \frac{d}{dt} f_{i_1 i_2, \mathbf{k}}^e &= \frac{1}{i\hbar} (\epsilon_{i_2, \mathbf{k}}^e - \epsilon_{i_1, \mathbf{k}}^e) f_{i_1 i_2, \mathbf{k}}^e \\ &+ \frac{1}{i\hbar} \sum_{j_1} (\mathcal{U}_{i_2 j_1, \mathbf{k}} p_{j_1 i_1, \mathbf{k}}^* - \mathcal{U}_{i_1 j_1, \mathbf{k}}^* p_{j_1 i_2, \mathbf{k}}), \end{aligned} \quad (14a)$$

$$\begin{aligned} \frac{d}{dt} f_{j_1 j_2, -\mathbf{k}}^h &= \frac{1}{i\hbar} (\epsilon_{j_2, -\mathbf{k}}^h - \epsilon_{j_1, -\mathbf{k}}^h) f_{j_1 j_2, -\mathbf{k}}^h \\ &+ \frac{1}{i\hbar} \sum_{i_1} (\mathcal{U}_{i_1 j_2, \mathbf{k}} p_{j_1 i_1, \mathbf{k}}^* - \mathcal{U}_{i_1 j_1, \mathbf{k}}^* p_{j_2 i_1, \mathbf{k}}), \end{aligned} \quad (14b)$$

$$\frac{d}{dt} p_{j_1 i_1, \mathbf{k}} = \frac{1}{i\hbar} (\epsilon_{j_1, -\mathbf{k}}^h + \epsilon_{i_1, \mathbf{k}}^e) p_{j_1 i_1, \mathbf{k}} + \mathcal{U}_{i_1 j_1, \mathbf{k}}. \quad (14c)$$

In this approximation, Eq. (14c) is independent of Eqs. (14a) and (14b). It describes unbound and bound electron-hole pairs, i.e., excitons. The solution of this equation then enters as source terms for Eqs. (14a) and (14b), which describe the generation of carrier populations in the subbands as well as a coherence in the electron and hole system, respectively.

III. RESULTS

The calculations have been performed for an $\text{Al}_x\text{Ga}_{1-x}\text{As}$ asymmetric double quantum well structure as shown in Fig. 1. Note that the energies of the various states in Fig. 1 are shifted arbitrarily to separate the plots of the wave functions. The well widths are 15 nm and 10 nm, the barrier width is 2.5 nm, and the Al fraction x of the barrier regions is 0.2. The parameters are taken in agreement with the experiments in Ref. 24. Using such a small barrier width, we are in the so-called “strong-coupling limit.”¹⁷ The interesting point in the

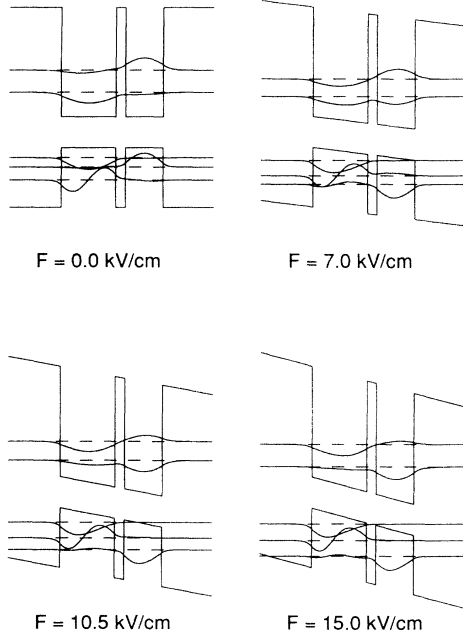


FIG. 1. Envelope wave functions of the asymmetric double quantum well for four values of the applied electric field. The well widths are 15 nm and 10 nm, the barrier width is 2.5 nm.

case of coupled quantum wells is the fact that the localization of the carriers can be controlled by an external electric field applied in the growth direction.

The pair energies of free electron-hole pairs at the subband edges, i.e., the energies connecting the three hole subband edges with the two electron subband edges ($\epsilon_{i,0}^e + \epsilon_{j,0}^h$), are shown as lines in Fig. 2 as functions of the applied electric field. The solid and the dashed lines refer to the transition from the first hole subband to the first and second electron subband. The anticrossing behavior at a field of 7 kV/cm is clearly visible. The dotted and dash-dotted lines refer to transitions from the second and the remaining two lines to transitions from the third hole

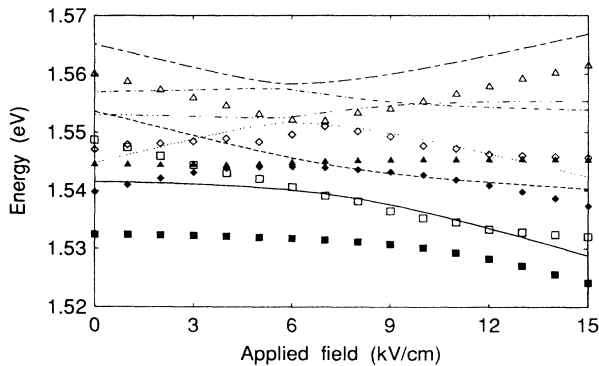


FIG. 2. Transition energies between the electron and hole subband edges (lines) and corresponding 1s exciton energies (symbols) calculated for two electron and three hole subbands (see Fig. 1).

subband into the two electron subbands, respectively.

Up to now Coulomb effects have not been taken into account. In the next section, we will include electron-hole interaction in the calculation of pair states, i.e., we calculate the excitonic eigenstates.^{14,15,41}

A. Exciton states

Since the interband polarization agrees with the electron-hole pair wave function in the (i, j, \mathbf{k}) space, with the ansatz⁴²

$$p_{j_1 i_1, \mathbf{k}} = \sum_n \tilde{p}_{j_1 i_1, \mathbf{k}}^{(n)} \exp(-i\omega_n t), \quad (15)$$

we obtain the eigenvalue equation

$$\begin{aligned} \hbar\omega_n \tilde{p}_{j_1 i_1, \mathbf{k}}^{(n)} = & (\epsilon_{j_1, -\mathbf{k}}^h + \epsilon_{i_1, \mathbf{k}}^e) \tilde{p}_{j_1 i_1, \mathbf{k}}^{(n)} \\ & - \sum_{i_2, j_2} \sum_{\mathbf{k}'} V_{i_1 j_2 j_1 i_2}(\mathbf{k} - \mathbf{k}') \tilde{p}_{j_2 i_2, \mathbf{k}'}^{(n)}. \end{aligned} \quad (16)$$

The eigenvalue $E_n = \hbar\omega_n$ is the exciton energy of state n and the corresponding eigenvector $\tilde{p}_{j_1 i_1, \mathbf{k}}^{(n)}$ is the exciton wave function in the (i, j, \mathbf{k}) space. The real space exciton wave function is then obtained by a unitary transformation using the electron and hole wave functions according to

$$\Phi^{(n)}(z_e, z_h; \mathbf{r}) = \frac{1}{\sqrt{A}} \sum_{i_1, j_1} \sum_{\mathbf{k}} \tilde{p}_{j_1 i_1, \mathbf{k}}^{(n)} e^{i\mathbf{k} \cdot \mathbf{r}} \phi_{i_1}(z_e) \phi_{j_1}(z_h), \quad (17)$$

where z_e (z_h) denote the electron (hole) z coordinate and \mathbf{r} the electron-hole relative coordinate in the xy plane.

Equation (16) has been solved numerically for the case of radially symmetric (s like) excitons on a discretized mesh in \mathbf{k} space for the asymmetric double-quantum-well structure shown in Fig. 1. Two electron and three hole subbands and 200 equidistant k values have been taken into account. The accuracy has been checked by performing the same numerical solution for the three- and two-dimensional limits, where the exciton energies are known analytically.

The symbols in Fig. 2 refer to the 1s-like exciton states corresponding to the transitions between the various subbands. It should be noted that for higher states the classification is not unique since these states are resonant with band-to-band transitions and, therefore, have no pure 1s behavior. We have plotted those states which exhibit the strongest 1s-like contribution in the wave function. In general, the field dependence of the exciton energies exhibits a similar behavior as the free-carrier energies; however, the resonance fields are shifted.^{14,15,24} Let us concentrate on the transitions from the first hole subband to the electron subbands (solid and dashed lines, solid and open squares). In the exciton case the resonance is shifted to a field of 10.5 kV/cm. The reason can be understood by looking at the binding energies in the low- and high-field limits. At low fields the open square

shows a larger binding energy than the solid square. This is due to the fact that in the former case electron and hole are localized in the same well (spatially direct exciton), while in the latter case they are localized in different wells (spatially indirect exciton) and thus have a reduced Coulomb interaction. On the other hand, at high fields the situation is reversed. This transition leads to the observed shift of the resonance.^{14,15,24} Similar shifts can be seen for the transitions including higher hole subbands.

These shifts of the resonance field are associated with a change in the localization behavior when going from noninteracting pair states to exciton states. The localization of an exciton state can be analyzed by plotting the pair density $\rho^{(n)}$ of the n th exciton state in the space of the electron and hole z coordinate. It is obtained from the real space exciton wave function $\Phi^{(n)}(z_e, z_h; \mathbf{r})$ by projection onto the (z_e, z_h) plane according to

$$\begin{aligned} \rho^{(n)}(z_e, z_h) &= \int_A |\Phi^{(n)}(z_e, z_h; \mathbf{r})|^2 d^2r \\ &= \sum_{\mathbf{k}} \left| \sum_{i_1, j_1} \tilde{p}_{j_1 i_1, \mathbf{k}}^{(n)} \phi_{i_1}(z_e) \phi_{j_1}(z_h) \right|^2. \end{aligned} \quad (18)$$

In Fig. 3 we report the projected pair density for the lowest exciton state at four values of the applied electric field. At zero field only one component of the wave function, in the present case p_{11} , is essentially nonzero; the exciton corresponds to one electron and one hole subband. Both electron and hole are localized in the wide well. At a field of 7 kV/cm the free electron states are in resonance and, therefore, they are delocalized (see Fig. 1). The exciton, however, is still almost completely localized in the wide well. At the exciton resonance field of 10.5 kV/cm, the electron contribution in the exciton state is completely delocalized. This is in contrast to the free-carrier states, which are out of resonance at this electric field. Finally, at a field of 15 kV/cm the electron is localized in the narrow well and the hole is localized in the wide well. We have a spatially indirect exciton. As in the case of zero field, only p_{11} is essentially nonzero.

B. Absorption spectra

The classification of exciton states related to higher subbands as obtained from a numerical diagonalization

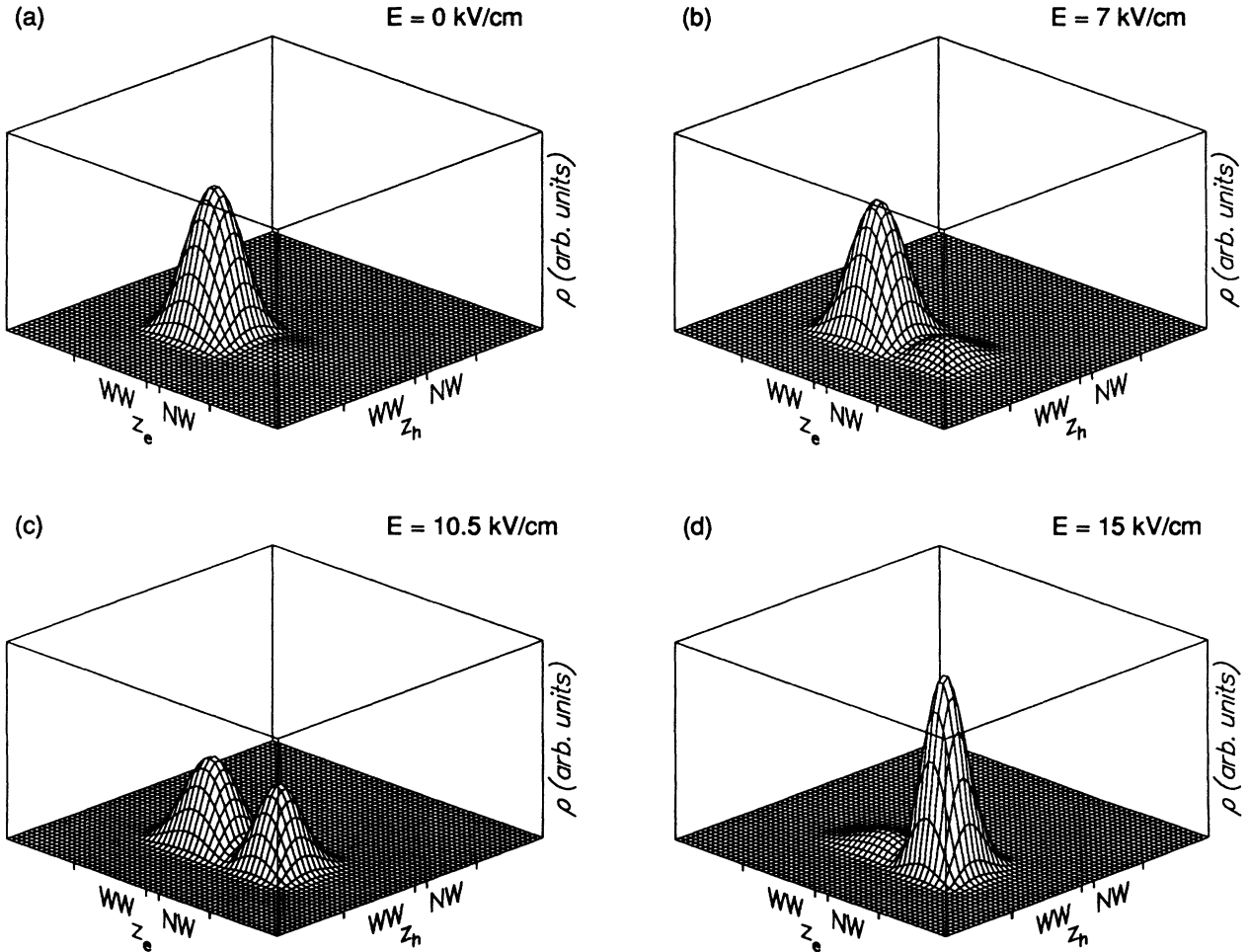


FIG. 3. Electron-hole pair-density [see Eq. (18)] along the growth direction for the lowest exciton state for four values of the applied electric field.

is usually not unique due to a coupling among different subbands and a mixing between discrete and continuum contributions. The excitonic states are eigenstates of the isolated system and, therefore, cannot be measured directly. To compare the results with an experiment, the coupling to the environment has to be taken into account. From the coupling to a classical light field the absorption spectrum can be calculated.^{42,37} In contrast to the classification of the excitonic states in Sec. III A, the absorption spectrum as an observable quantity is unique.

To calculate the absorption spectrum, we expand the interband polarization in the exciton basis according to

$$p_{j_1 i_1, \mathbf{k}} = \sum_n \tilde{p}_{j_1 i_1, \mathbf{k}}^{(n)} B_n, \quad (19)$$

with expansion coefficients B_n . The corresponding exciton dipole matrix element is given by

$$\mathbf{M}_n = \sum_{i_1, j_1} \sum_{\mathbf{k}} \tilde{p}_{j_1 i_1, \mathbf{k}}^{(n)*} \mathbf{M}_{i_1 j_1, \mathbf{k}}^{eh}. \quad (20)$$

The absorption spectrum is then given by a sum of absorption peaks at the exciton energies, the strength of each peak being proportional to the square of the dipole matrix element. The broadening of the peaks can be either due to dephasing leading to a Lorentzian shape or, if measured with a laser pulse shorter than the dephasing time, due to the energetic width of the pulse, leading to a line shape according to the laser pulse. Here, we consider this second case by assuming a Gaussian pulse with a duration τ_L and central angular frequency ω_L and obtain for the absorbed intensity $I(\omega_L)$ of the pulse,

$$I(\omega_L) = \frac{\pi \tau_L^2}{\hbar^2} \sum_n (\mathbf{M}_n \cdot \mathbf{e}_L)^2 E_L^2 \exp \left[-\frac{1}{2} \tau_L^2 (\omega_n - \omega_L)^2 \right]. \quad (21)$$

In Fig. 4, we have plotted the absorption spectrum $I(\omega_L)$ of a 1 ps Gaussian pulse as a function of the photon energy $\hbar\omega_L$ and the applied electric field E . Without the applied field, we observe two strong peaks corresponding to the p_{11} and the p_{22} exciton which are both direct excitons. In between these two peaks is a weak peak corresponding to the indirect p_{21} exciton which can be excited due to the nonvanishing contribution of the lowest electron state in the narrow well (see Fig. 1). At the highest field of 15 kV/cm we observe two strong peaks, now related to the direct p_{12} and the p_{31} excitons, and two weak peaks due to the indirect p_{11} and p_{32} exciton. When going from low to high fields, the anticrossing behavior associated with the change in the oscillator strength from one component to the other is clearly visible for both pairs of transitions, those belonging to the wide well hole state at lower energies and those belonging to the narrow well hole state at higher energies.

In our model, only s -like excitons are considered. Therefore, in our spectra there are no transitions due to valence band mixing of excitons which have p symmetry in the plane of the interfaces. Such transitions may gain significant oscillator strength. A detailed discussion

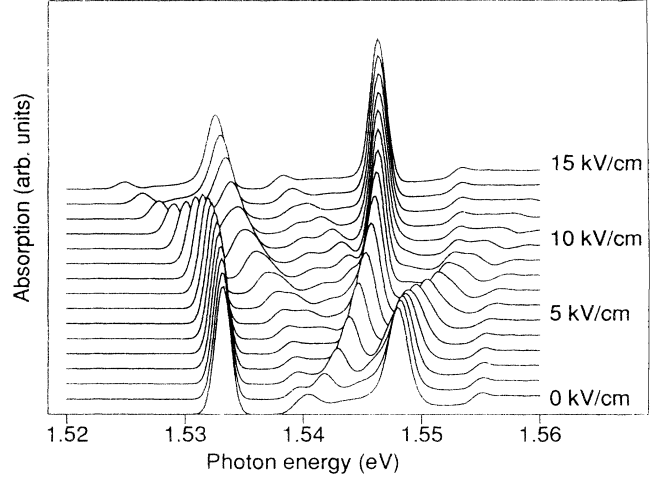


FIG. 4. Absorption spectra for a 1 ps pulse as function of the photon energy and the applied electric field.

of these effects can be found in Ref. 37.

The coherent dynamics in the following sections will be investigated in the case of the wide well resonance. Therefore, we will discuss in some more detail the absorption spectrum for the applied field of 10.5 kV/cm as plotted in Fig. 5. We observe two peaks of approximately the same strength at 1.530 eV and 1.534 eV, corresponding to the delocalized excitons, and a strong peak at 1.546 eV corresponding to the direct exciton in the narrow well. In the upper part of Fig. 5, we have indicated the positions of the excitons as obtained from the diagonalization, the length of the bars being proportional to the exciton dipole matrix elements. We see that the second peak has contributions from several exciton states which explains the larger width of this peak compared to the lowest peak. The corresponding exciton wave functions reveal that these states have a $1s$ -like contribution from the second subband and an n - s -like contribution ($n = 2, 3, \dots$) from the first subband, i.e., we observe a

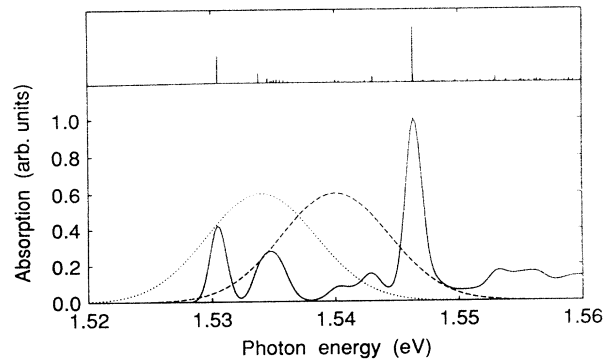


FIG. 5. Absorption spectrum for a 1 ps pulse as function of the photon energy at an applied electric field of 10.5 kV/cm. In the upper part the positions of the exciton states are indicated, the length of the bars being proportional to the exciton dipole matrix element.

mixing of the exciton ground state of the second subband with excited states from the first subband.

Experimentally the absorption spectrum can be obtained by measuring the photocurrent after excitation by a laser pulse with varying photon energy.²⁴ Such a situation can be modeled directly by solving the semiconductor Bloch equations for a laser pulse with fixed pulse duration and intensity but with varying photon energy and calculate the carrier density generated by this pulse as a function of the photon energy. The photocurrent will then be proportional to final density of carriers. Results obtained by this method have been given in Ref. 28. In the case of a sufficiently low laser intensity, we find a good agreement with the absorption spectrum calculated from the exciton states by using the matrix diagonalization. This demonstrates that for physically observable quantities both methods are numerically equivalent.

The calculated spectrum is in good agreement with the measured photocurrent spectrum (Fig. 2 in Ref. 24), except for the additional light hole peaks in the measured spectrum which, of course, are not present in the present calculations. In particular, the position and the relative strengths of the three main peaks are very well reproduced by the numerical simulation, thus confirming the reliability of the model and of the numerical solution. Therefore, it seems possible to neglect nonparabolicity and the effects of valence band mixing on the heavy holes.

C. Charge oscillations

When the spectral width of a laser pulse overlaps with two or more excitonic states which share a common electron or hole state, and both of them have a nonzero dipole matrix element, a linear combination of these excitons is generated. If the localization behavior of the states is different, the dynamics of such a wave packet is associated with a time-dependent charge density. Neglecting intraband contributions, which oscillate in the frequency range determined by the gap, the charge density $\rho(z, t) = -e[n^e(z, t) - n^h(z, t)]$ is given by

$$n^e(z, t) = \sum_{i_1, i_2} \sum_{\mathbf{k}} \phi_{i_1}^*(z) \phi_{i_2}(z) f_{i_1 i_2, \mathbf{k}}^e(t), \quad (22a)$$

$$n^h(z, t) = \sum_{j_1, j_2} \sum_{\mathbf{k}} \phi_{j_1}^*(z) \phi_{j_2}(z) f_{j_1 j_2, \mathbf{k}}^h(t). \quad (22b)$$

For the investigation of the dynamics, we include a phenomenological dephasing in the semiconductor Bloch equations characterized by a dephasing time T_2^{eh} for the interband polarization, a dephasing time T_2^{ee} for the electron intraband polarization, and a time T_2^{hh} for the hole interband polarization. The distribution functions $f_{i_1 i_2, \mathbf{k}}^e$ and $f_{j_1 j_2, \mathbf{k}}^h$ remain undamped. They decay only due to spontaneous emission processes which occur on a much longer time scale than considered here. The redistribution of carriers inside and between the subbands due to scattering processes is neglected in the present model.

The assumption of a relaxation time approximation with constant, \mathbf{k} -independent dephasing times is of

course a very crude approximation. One would expect that the dephasing times for continuum states will be considerably smaller than those for the lowest bound excitons.²⁹ However, this model allows us to concentrate on the role played by the various time constants.

Figure 6 shows the electron and hole densities for the case of an excitation with a 150 fs pulse at a photon energy of 1.54 eV and an applied electric field of 10.5 kV/cm as functions of time and the coordinate z in growth direction. A value of 3 ps has been taken for all three dephasing times. The spectral shape of the pulse is indicated by the dashed line in Fig. 5. We find a complex behavior due to the overlap of the pulse with many exciton states. In the case of the electron density, we observe a contribution which oscillates between the wells and a background density which is mainly localized in the narrow well. For the holes, we find a background in both wells and a superimposed oscillation inside the wide well. Let us now try to understand this behavior.

From Fig. 5, we see that there is large overlap with the strong peak at 1.546 eV. As explained above, this peak corresponds to a spatially direct exciton localized in the narrow well and is responsible for the hole density and the main part of the electron density in the narrow well. The oscillation in the electron density is related to the excitation of the two excitons with the hole localized in the wide well and the electrons delocalized over both wells. The oscillation in the hole density shows that there

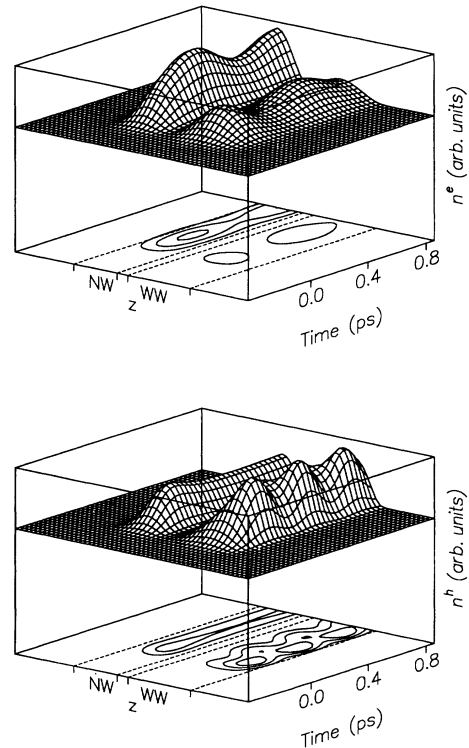


FIG. 6. (a) Electron density $n^e(z, t)$ and (b) hole density $n^h(z, t)$ as functions of the z coordinate and time for the case of an applied field of 10.5 kV/cm and an excitation with a 150 fs pulse at a photon energy of 1.54 eV.

is also a remarkable contribution from the excited hole state in the wide well which, as already discussed, showed up as a small peak in the absorption spectrum. The oscillation frequency of the holes is larger because the energy difference between the first and second hole state is larger than that one between the electron states. In the next section, we will discuss in detail the frequencies appearing in the dynamics.

D. Terahertz emission

According to classical electrodynamics, time-dependent charge densities as shown in Fig. 6 lead to the emission of an electromagnetic radiation. The far-field behavior is dominated by dipole radiation, the electric field strength being proportional to the second temporal derivative of the dipole moment. Such an emission due to oscillations in the terahertz range has recently been observed in various systems.^{21,23,24,27}

In the system studied here, the total dipole moment \mathbf{P} can be split into two parts, an interband part $\mathbf{P}^{\text{inter}}$ and an intraband part $\mathbf{P}^{\text{intra}}$, where

$$\mathbf{P}^{\text{inter}} = \sum_{i_1, j_1} \sum_{\mathbf{k}} (\mathbf{M}_{i_1 j_1}^{eh} p_{j_1 i_1, \mathbf{k}}^* - \mathbf{M}_{i_1 j_1}^{eh*} p_{j_1 i_1, \mathbf{k}}), \quad (23)$$

$$\mathbf{P}^{\text{intra}} = \sum_{i_1, i_2} \sum_{\mathbf{k}} \mathbf{M}_{i_1 i_2}^{ee} f_{i_1 i_2, \mathbf{k}}^e + \sum_{j_1, j_2} \sum_{\mathbf{k}} \mathbf{M}_{j_1 j_2}^{hh} f_{j_1 j_2, \mathbf{k}}^h, \quad (24)$$

with $\mathbf{P} = \mathbf{P}^{\text{inter}} + \mathbf{P}^{\text{intra}}$ and the intraband dipole matrix elements,

$$\begin{aligned} \mathbf{M}_{i_1 i_2}^{ee} &= -e \mathbf{e}_z \int \phi_{i_1}^*(z) z \phi_{i_2}(z) dz, \\ \mathbf{M}_{j_1 j_2}^{hh} &= e \mathbf{e}_z \int \phi_{j_1}^*(z) z \phi_{j_2}(z) dz, \end{aligned} \quad (25)$$

where \mathbf{e}_z denotes a unit vector in z direction. The interband part oscillates in the frequency range determined by the gap energy and, therefore, leads to an emission in the visible spectral range. This effect is the basis for four-wave-mixing spectroscopy which, being a third-order effect in the light field, is present also in a homogeneous bulk semiconductor and will not be considered in this paper.

Here we are interested in the intraband part. It can be separated again into two parts, a part which is diagonal in the subband indices, and an off-diagonal part. A characteristic time for the change of the diagonal part, i.e., of the distribution functions, is given by the pulse shape of the laser. If electron and hole states are localized in different regions in space, a net dipole moment builds up which gives rise to the so-called “optical rectification pulse,” as may occur in the case of excitation in the region of a built-in field close to a surface.²⁰ In addition, if the energetic width of a laser pulse is larger than the difference between two subbands, a coherent superposition of states belonging to both subbands is generated, as has been discussed in the previous section. The charge oscillation corresponds to the creation of intra-

band polarizations and, thus, to an off-diagonal part in the intraband dipole moment which oscillates in the frequency range determined by the energy splitting of the subbands and leads to the emission of a coherent terahertz radiation.^{21,24,23}

In Fig. 7(a), the intraband dipole moment is plotted as a function of time for the case of the charge oscillations shown in Fig. 5. We see the build up of a dipole moment due to the different localizations of electrons and holes. At short times, this build up is accompanied by oscillations which decay with the dephasing times taken as 3 ps. The oscillatory part of the dipole moment is mainly governed by the oscillations of the electrons, superimposed we see the structure related to the oscillations of the holes. Figure 7(b) shows the second time derivative of the dipole moment which is proportional to the emitted signal. Here, the holes are responsible for the dominant structure due to their frequency, which is about a factor of 2 larger than that of the electrons.

Figure 8(a) shows the spectral intensity of the emitted signal, i.e., the absolute square of the Fourier transformed signal. The two peaks corresponding to the oscillations of electrons between the wells and of holes inside the wide well are clearly visible. It is interesting to notice that the calculated oscillation frequency of the lower peak of 1.57 THz corresponding to an energy of 6.5 meV is in very good agreement with the experiment.²⁴ This confirms that our model includes the most important features of the experiment. The oscillation frequency is remarkably larger than the splitting of the two lowest peaks in the absorption spectrum (3.5 meV) as would be the expected emission frequency due to a superposition of exciton states in a three-level model.

We will not try to compare quantitatively the calculated shape of the spectra with the experiment. This

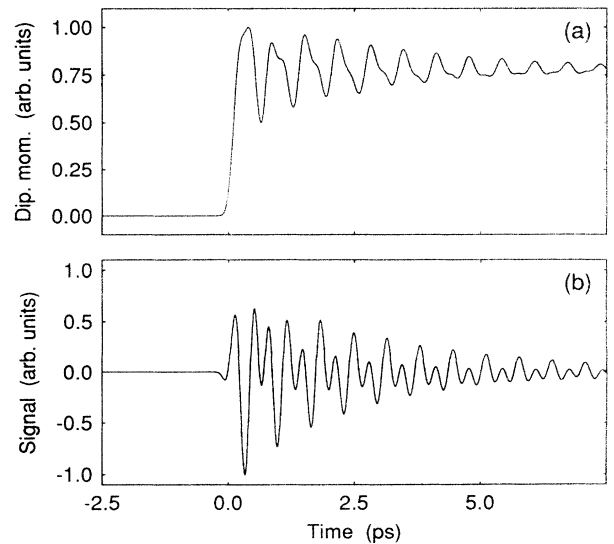


FIG. 7. (a) Dipole moment and (b) emitted signal of the asymmetric double-quantum-well system as functions of time for the case of excitation with a 150 fs pulse at 1.54 eV and an applied electric field $E = 10.5$ kV/cm.

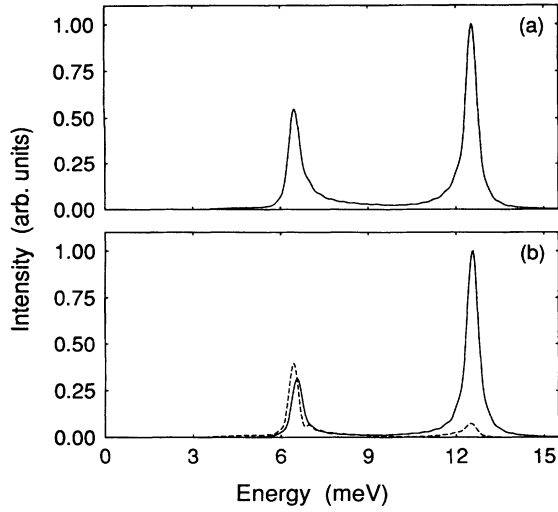


FIG. 8. (a) Spectral intensity of the emitted signal in Fig. 7 and (b) spectral intensities of the separate contributions driven directly by the field (solid line) and driven by exciton-exciton interaction (dashed line).

would require us to take into account the response function of the antenna, which usually increases the rectification part at low frequencies and strongly reduces the high frequency peak. Furthermore, different dephasing times for exciton ground states, excited states, and continuum states should be taken into account.²⁹ Our main objective is to investigate the various contributions entering the emitted signal and to analyze the role of the dephasing rates in determining the relevant contributions. Therefore, we limit ourselves to the simple dephasing model with only three time constants.

To obtain a better understanding of the emission process and of the frequencies involved, we transform the interband polarization into the exciton representation according to Eq. (19). In the case of parabolic bands, as considered here, the splitting between different subbands is independent of the in-plane wave vector \mathbf{k} . Under this condition, we can write down equations of motion directly for the intraband dipole moments,

$$\mathbf{P}_{i_1 i_2}^e = \sum_{\mathbf{k}} \mathbf{M}_{i_1 i_2}^{ee} f_{i_1 i_2, \mathbf{k}}^e, \quad (26a)$$

$$\mathbf{P}_{j_1 j_2}^h = \sum_{\mathbf{k}} \mathbf{M}_{j_1 j_2}^{hh} f_{j_1 j_2, -\mathbf{k}}^h. \quad (26b)$$

Starting from Eqs. (14) and (16), we obtain the equations of motion

$$\begin{aligned} \frac{d}{dt} \mathbf{P}_{i_1 i_2}^e &= \left(-i\omega_{i_1 i_2}^e - \frac{1}{T_2^{ee}}(1 - \delta_{i_1 i_2}) \right) \mathbf{P}_{i_1 i_2}^e \\ &+ \sum_n \left[\alpha_{i_1 i_2}^{e(n)} E^{(+)}(t) B_n^* + \alpha_{i_2 i_1}^{e(n)*} E^{(-)}(t) B_n \right] \\ &+ \sum_{n, n'} \left[\beta_{i_1 i_2}^{e(n, n')} B_n^* B_{n'} + \beta_{i_2 i_1}^{e(n, n')*} B_n B_{n'}^* \right], \end{aligned} \quad (27a)$$

$$\begin{aligned} \frac{d}{dt} \mathbf{P}_{j_1 j_2}^h &= \left(-i\omega_{j_1 j_2}^h - \frac{1}{T_2^{hh}}(1 - \delta_{j_1 j_2}) \right) \mathbf{P}_{j_1 j_2}^h \\ &+ \sum_n \left[\alpha_{j_1 j_2}^{h(n)} E^{(+)}(t) B_n^* + \alpha_{j_2 j_1}^{h(n)*} E^{(-)}(t) B_n \right] \\ &+ \sum_{n, n'} \left[\beta_{j_2 j_1}^{h(n, n')} B_n^* B_{n'} + \beta_{j_1 j_2}^{h(n, n')*} B_n B_{n'}^* \right], \end{aligned} \quad (27b)$$

$$\frac{d}{dt} B_n = \left(-i\omega_n - \frac{1}{T_2^{eh}} \right) B_n + \frac{1}{i\hbar} \mathbf{M}_n \cdot \mathbf{e}_L E^{(+)}(t), \quad (27c)$$

with $\hbar\omega_{i_1 i_2}^e = (\epsilon_{i_2, \mathbf{k}}^e - \epsilon_{i_1, \mathbf{k}}^e)$, $\hbar\omega_{j_1 j_2}^h = (\epsilon_{j_2, \mathbf{k}}^h - \epsilon_{j_1, \mathbf{k}}^h)$, and

$$\alpha_{i_1 i_2}^{e(n)} = \frac{1}{i\hbar} \mathbf{M}_{i_1 i_2}^{ee} \sum_{j_1} \sum_{\mathbf{k}} (\mathbf{M}_{i_2 j_1, \mathbf{k}}^{eh} \cdot \mathbf{e}_L) \tilde{p}_{j_1 i_1, \mathbf{k}}^{(n)*}, \quad (28a)$$

$$\alpha_{j_1 j_2}^{h(n)} = \frac{1}{i\hbar} \mathbf{M}_{j_1 j_2}^{hh} \sum_{i_1} \sum_{\mathbf{k}} (\mathbf{M}_{i_1 j_2, \mathbf{k}}^{eh} \cdot \mathbf{e}_L) \tilde{p}_{j_1 i_1, \mathbf{k}}^{(n)*}, \quad (28b)$$

$$\begin{aligned} \beta_{i_1 i_2}^{e(n, n')} &= \frac{1}{i\hbar} \mathbf{M}_{i_1 i_2}^{ee} \sum_{j_1} \sum_{\mathbf{k}} (E_{n'} - \epsilon_{i_2, \mathbf{k}}^e \\ &- \epsilon_{j_1, -\mathbf{k}}^h) \tilde{p}_{j_1 i_2, \mathbf{k}}^{(n')} \tilde{p}_{j_1 i_1, \mathbf{k}}^{(n)*}, \end{aligned} \quad (28c)$$

$$\begin{aligned} \beta_{j_1 j_2}^{h(n, n')} &= \frac{1}{i\hbar} \mathbf{M}_{j_1 j_2}^{hh} \sum_{i_1} \sum_{\mathbf{k}} (E_{n'} - \epsilon_{i_1, \mathbf{k}}^h \\ &- \epsilon_{j_2, -\mathbf{k}}^h) \tilde{p}_{j_2 i_1, \mathbf{k}}^{(n')} \tilde{p}_{j_1 i_1, \mathbf{k}}^{(n)*}. \end{aligned} \quad (28d)$$

Here we have included the three dephasing times describing the decay of the intraband and interband polarizations. All three equations have the structure of driven, damped harmonic oscillators. Equation (27c) describes the dynamics of the exciton state n . The exciton amplitude B_n is created by the laser pulse and, after the pulse has finished, it oscillates with its eigenfrequency ω_n and decays with the interband dephasing time. Equations (27a) and (27b) have source terms of two different types: First, there are terms involving the direct coupling of the external light field $\mathbf{E}(t)$ to the excitons. As in the interband case, these terms vanish after the pulse and lead to a damped oscillation of the intraband polarizations with a frequency corresponding to the subband splitting of noninteracting carriers and a decay time given by the intraband dephasing times. The second type of driving terms is due to exciton-exciton interaction and is described by products $B_n^* B_{n'}$. These source terms have characteristic frequencies $(E_{n'} - E_n)/\hbar$ and are present also after the pulse. Therefore, if the pulse excites several exciton states due to a sufficiently large bandwidth, the intraband polarizations are driven with the frequency of the quantum beats between these states. These driving terms decay with the time $2T_2^{eh}$. If this decay time is sufficiently large compared to the intraband dephasing time, the driving term will determine the oscillation frequency of the intraband polarizations and we will expect a radiation with the beat frequency of the excitons. If, on the other hand, the interband decay time is shorter than the intraband times, the intraband polarizations will exhibit mainly a damped oscillation with the frequency of the subband splitting. If neither of these limiting cases

is reached, in general, exciton as well as free-carrier frequencies will contribute to the dynamics and, therefore, to the spectrum of the terahertz radiation. The spectral shape will then strongly depend on the details of the excitation conditions.

Since Eqs. (27a), (27b) are linear in the intraband polarizations, we can separate the emitted signal in two parts. This is shown in Fig. 8(b). The solid line refers to the contribution induced by source terms involving the light field [terms with coefficients α in Eqs. (27)]. We see two peaks at the free-carrier energy differences between the electron subbands and between the first and the second hole subband. There are no frequencies involving the third hole subband because the intersubband dipole matrix elements with this subband are negligible due to the nearly complete localization of the hole states in either the wide or the narrow well (see Fig. 1). The dashed line refers to the contributions due to the exciton-exciton driving terms [terms with coefficients β in Eqs. (27)]. It turns out that also this part is dominated by the free-carrier frequencies. The reason is that the exciton-exciton driving term decays with $T_2^{eh}/2 = 1.5$ ps, which is faster than the intraband dephasing. However, in the dashed line, we notice a slight contribution below the resonance peak which is related to excitonic beating energies.

This interpretation of the various frequencies entering the spectrum of THz emission can be checked by changing the dephasing times. For this purpose, we will now compare the case of equal times with the cases where one of the times, the interband or the intraband dephasing time, is much shorter than the other. In order to concentrate on the most interesting part of the spectrum in the region of the exciton resonance, we study the case of an excitation between the two resonant exciton peaks at a photon energy of 1.534 eV. This reduces the contribution due to oscillations in the hole system. Figure 9 shows the spectra of the emitted radiation (left column) and the corresponding decomposition (right column) with respect to the different driving terms for three combinations of interband and intraband dephasing times. Figures 9(a) and 9(b) are obtained with the same values as above, $T_2^{eh} = T_2^{ee} = T_2^{hh} = 3$ ps. Compared to the previous case, now the low frequency part of the spectrum is increased. However, the spectrum is still dominated by the energy splitting of the free electron states. This effect is further increased by reducing the interband dephasing time to a value of $T_2^{eh} = 0.6$ ps and keeping fixed the intraband times. Now both driving terms act effectively as a short impact for the intraband oscillators, which then oscillate with their characteristic frequencies. The contribution below the 6.5 meV resonance related to the exciton beating, which was visible in Fig. 9(a), has now vanished. If, on the other hand, we reduce the intraband dephasing times to $T_2^{ee} = T_2^{hh} = 0.5$ ps and increase the interband dephasing time to $T_2^{eh} = 8$ ps, the exciton driving term decays much slower than the free-carrier oscillations. The line in Fig. 9(e) is now concentrated at the exciton splitting energy of 3.5 meV. The superimposed slight structure is related to the fact that, as has been discussed above, the exciton related to the second elec-

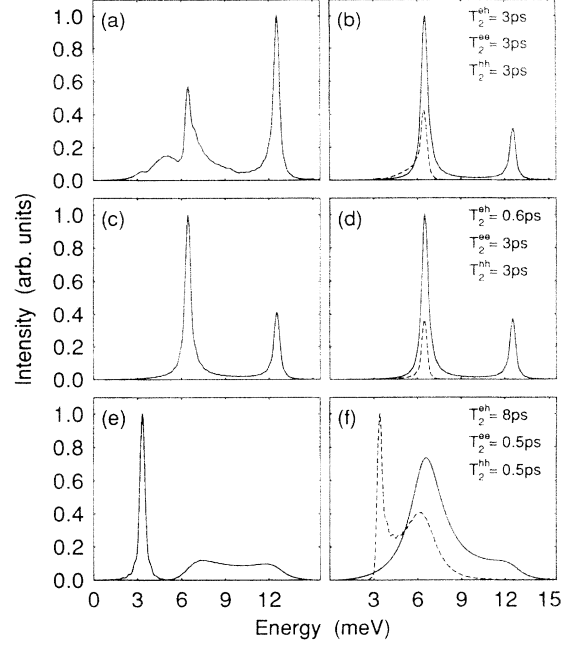


FIG. 9. (a),(c),(e) spectral intensity of the emitted signal and (b),(d),(f) separate contributions as in Fig. 8 for the case of excitation with a 150 fs pulse at 1.534 eV and an applied electric field $E = 10.5$ kV/cm for different combinations of interband and intraband dephasing times.

tron subband mixes with excited states of the exciton from the first subband leading to several contributions with similar oscillator strength (see Fig. 5).

IV. CONCLUSION

We have presented an analysis of eigenstates, coherent dynamics, and terahertz-emission in an asymmetric double quantum well. The theory has been based on the semiconductor Bloch equations in the low-density case, which have been solved numerically. We have calculated exciton energies and eigenfunctions in asymmetric double quantum wells as functions of an applied electric field. For varying electric field, the localization behavior of the excitonic states changes, leading to a transition from spatially direct to spatially indirect excitons, the resonance field, however, is shifted with respect to the resonance field for free-carrier states. From these data, we have calculated absorption spectra which are in good agreement with experiments.

We then have investigated the coherent dynamics induced by a laser pulse. For the case of carrier generation in a superposition of states, we have calculated the coherent emission of a terahertz radiation. The dynamics has been analyzed both in a free-carrier and an exciton representation. The latter one has allowed us to individuate two different contributions leading to oscillations either with the free-carrier subband splitting or with exciton beating frequencies. The spectral shape of the emitted signal depends on details of the dephasing mechanisms, in

particular, on the ratio between interband and intraband dephasing times. The calculations, therefore, explain the difference between the splitting of excitonic absorption lines and the frequency of terahertz emission as observed experimentally.

ACKNOWLEDGMENTS

This work has been supported in part by the Deutsche Forschungsgemeinschaft (SFB 329). We thank H. G. Roskos and C. Waschke for valuable discussions.

- ¹ L. Schultheis, M. D. Sturge, and J. Hegarty, *Appl. Phys. Lett.* **47**, 995 (1985).
- ² P. C. Becker *et al.*, *Phys. Rev. Lett.* **61**, 1647 (1988).
- ³ G. Noll, U. Siegner, S. G. Shevel, and E. O. Göbel, *Phys. Rev. Lett.* **64**, 792 (1990).
- ⁴ M. Lindberg, R. Binder, and S. W. Koch, *Phys. Rev. A* **45**, 1865 (1992).
- ⁵ A. Lohner *et al.*, *Phys. Rev. Lett.* **71**, 77 (1993).
- ⁶ K. Leo *et al.*, *Appl. Phys. Lett.* **57**, 19 (1990).
- ⁷ E. O. Göbel *et al.*, *Phys. Rev. Lett.* **64**, 1801 (1990).
- ⁸ V. Langer, H. Stolz, and W. von der Osten, *Phys. Rev. Lett.* **64**, 854 (1990).
- ⁹ J. Feldmann *et al.*, *Phys. Rev. Lett.* **70**, 3027 (1993).
- ¹⁰ K. Leo *et al.*, *Appl. Phys. Lett.* **56**, 2031 (1990).
- ¹¹ D.-S. Kim *et al.*, *Phys. Rev. Lett.* **69**, 2725 (1992).
- ¹² S. Weiss *et al.*, *Phys. Rev. Lett.* **69**, 2685 (1992).
- ¹³ W. Schäfer, F. Jahnke, and S. Schmitt-Rink, *Phys. Rev. B* **47**, 1217 (1993).
- ¹⁴ G. Bastard, C. Delalande, R. Ferreira, and H. W. Liu, *J. Lumin.* **44**, 247 (1989).
- ¹⁵ A. M. Fox *et al.*, *Phys. Rev. B* **44**, 6231 (1991).
- ¹⁶ A. P. Heberle, W. W. Rühle, M. G. W. Alexander, and K. Köhler, *Semicond. Sci. Technol.* **7**, B421 (1992).
- ¹⁷ R. Ferreira *et al.*, *Phys. Rev. B* **45**, 11782 (1992).
- ¹⁸ K. Leo *et al.*, *Phys. Rev. B* **44**, 5726 (1991).
- ¹⁹ X.-C. Zhang, Y. Jin, and X. F. Ma, *Appl. Phys. Lett.* **61**, 2764 (1992).
- ²⁰ S. L. Chuang *et al.*, *Phys. Rev. Lett.* **68**, 102 (1992).
- ²¹ P. C. M. Planken *et al.*, *Phys. Rev. Lett.* **69**, 3800 (1992).
- ²² I. Brener *et al.*, *Appl. Phys. Lett.* **63**, 2213 (1993).
- ²³ M. C. Nuss *et al.*, *Appl. Phys. B* **58**, 249 (1994).
- ²⁴ H. G. Roskos *et al.*, *Phys. Rev. Lett.* **68**, 2216 (1992).
- ²⁵ P. C. M. Planken *et al.*, *Phys. Rev. B* **48**, 4903 (1993).
- ²⁶ M. S. C. Luo *et al.*, *Phys. Rev. B* **48**, 11043 (1993).
- ²⁷ C. Waschke *et al.*, *Phys. Rev. Lett.* **70**, 3319 (1993).
- ²⁸ T. Kuhn *et al.*, in *Proceedings of the NATO Advanced Research Workshop "Coherent Optical Interactions in Semiconductors," 1993*, NATO Advanced Study Institute, Series B: Physics, edited by R. T. Phillips (Plenum, New York, in press).
- ²⁹ When completing this manuscript we learned that, by using a similar model, C. Chansungsan, L. Tsang, and S. L. Chuang, *J. Opt. Soc. Am. B* (to be published) have been able to fit to the experimental data by using energy-dependent phenomenological dephasing rates.
- ³⁰ L. Tsang, C. Chansungsan, and S. L. Chuang, *Phys. Rev. B* **45**, 11918 (1992).
- ³¹ Y. Z. Hu, R. Binder, and S. W. Koch, *Phys. Rev. B* **47**, 15679 (1993).
- ³² S. Schmitt-Rink and D. S. Chemla, *Phys. Rev. Lett.* **57**, 2752 (1986).
- ³³ S. Schmitt-Rink, D. S. Chemla, and H. Haug, *Phys. Rev. B* **37**, 941 (1988).
- ³⁴ M. Lindberg and S. W. Koch, *Phys. Rev. B* **38**, 3342 (1988).
- ³⁵ T. Kuhn and F. Rossi, *Phys. Rev. Lett.* **69**, 977 (1992).
- ³⁶ T. Kuhn and F. Rossi, *Phys. Rev. B* **46**, 7496 (1992).
- ³⁷ C. Y.-P. Chao and S. L. Chuang, *Phys. Rev. B* **48**, 8210 (1993).
- ³⁸ R. Winkler and U. Rössler, *Phys. Rev. B* **48**, 8918 (1993).
- ³⁹ H. Haken, *Quantum Field Theory of Solids, An Introduction* (North-Holland, New York, 1976).
- ⁴⁰ H. Haug, in *Optical Nonlinearities and Instabilities in Semiconductors*, edited by H. Haug (Academic, San Diego, 1988), p. 53.
- ⁴¹ L. C. Andreani and A. Pasquarello, *Phys. Rev. B* **42**, 8928 (1990).
- ⁴² S.-L. Chuang, S. Schmitt-Rink, D. A. B. Miller, and D. S. Chemla, *Phys. Rev. B* **43**, 1500 (1991).